Additive Manufacturing of Tungsten Heavy Alloys – A Technology Assessment of sinter-based AM Processes

Dirk HANDTRACK[1]*, Lukas PARTNER[1], Rafael CURY[2], Pascal MAHOT[2] and Bernhard MAYR-SCHMOELZER[1]

[1]Plansee SE, Metallwerk-Plansee-Str. 71, Reutte, 6600, Austria.
[2]Plansee Tungsten Alloys, la marque de CIME BOCUZE S.A.S., 446 Avenue des Digues, Saint Pierre en Faucigny, 74800, France

Abstract
Additive manufacturing (AM) of metals has undergone rapid technological development over the past 2 decades. While the beginning was strongly influenced by the development of beam-based processes, the sinter-based AM processes have gained more and more diversity and importance for more than 5 years now. This review presents the results of investigations following process developments of selected sinter-based AM processes using elemental powder mixtures to produce WHA parts. The achieved sintering densities, microstructures, purities as well as mechanical properties are compared with the minimum requirements of the current ASTM standard B777 and typical values of the conventional PM route (p/s). Manufactured demonstrators show the advantages and opportunities of the technologies. According to the current state of technical knowledge, a concluding process overview should serve as a decision-making aid for the right choice of technology for the additive manufacturing of WHA products, considering selected criteria as well as the limitations.

Keywords: Additive manufacturing, tungsten heavy alloys, properties.

Introduction
Tungsten heavy alloys (WHAs) are composite materials consisting of a major amount of spherical tungsten grains in a body-centered cubic (bcc) crystal lattice (α phase) surrounded by a Nickel based face-centered cubic (fcc) binder phase (called γ), containing several alloying elements in solid solution such as Fe, Co, Mo, besides W itself. Manufactured using powder metallurgy, fully consolidated WHAs are obtained through solid-liquid sintering under hydrogen. Indeed, the monocrystalline spherical bcc W nodules are the result of the reduction of the W/liquid interface energy and the coalescence of W particles by Ostwald ripening. The high density observed in these materials and their interesting thermal properties enable the use of these alloys as thermal resistant materials. Their microstructure is suitable for plastic deformation. Consequently, these materials can be used for a plethora of applications such as die casting molds, pins, sprue brushes as well as balancing weights for aerospace and automative parts. With the improvement of characteristics throughout the years, these materials are also suitable for ammunition applications such as Kinetic Energy Penetrators. It is then not surprising that there is a rising interest on using 3D printing approaches to obtain parts out of those alloys. Similarly to other materials, the advantages of additive manufacturing are (near)-net shape manufacturing, saving costs on prime materials, as well as gaining additional design freedom.
There is some literature [1-4] on the processing of WHAs via laser beam-based additive manufacturing (LBAM) such as Laser Powder Bed Fusion (LPBF) or Laser Metal Deposition (LMD). The flowability of the powders required in these processes was achieved by means of special, coarse powders (e.g. atomized powders, pre-mixed with coarse W powders or mechanically alloyed powders). The authors report on the formation of a microstructure with dendritic W precipitates and undesirable intermetallic phases as well as on the evaporation of parts of the metallic Ni-Fe phase in the printing process because of high energy inputs. The reported densities were mostly well below the theoretical density of the materials and the samples were largely brittle. Only a subsequent heat treatment at 1500°C, which is very close to a typical liquid-phase sintering of WHA, led to typical microstructures, which also resulted in a more ductile material behavior. Studnitzky et al. give a good overview of many different sinter-based AM methods (SBAM) independent of the processed material [5]. In very general terms, the advantages and disadvantages of the individual methods are compared there. Many of these SBAM processes offer a more suitable workflow than the LBAM processes specifically for WHAs, because the resulting microstructure is the same as when conventional manufacturing techniques are used.
In the present work, selected sinter-based AM processes were examined for their suitability to process an element powder mixture of WHA Densimet® D185, a WHA with a high content of tungsten. The alloy contains 97 wt.% W, 2 wt.% Ni and 1 wt.% Fe and corresponds to Class 4 tungsten heavy alloy by ASTM standard B777-15 [6]. Table 1 shows the minimum requirements of this alloy according to this standard.

*corresponding author, E-mail: dirk.handtrack@plansee.com

Table 1: Minimum requirements of WHA D185 according to the ASTM B777-15 standard* and typical values of conventional manufacturing (p/s)

WHA class 4 (ASTM*)	tungsten, nominal wt.%	density in g/ccm	$R_{p0.2}$ in MPa	R_m in MPa	A in %
minimum requirements	97	18.25-18.85	517	689	2
typical values D185 (p/s)	97	18.52	735	985	15

Experimental

The technology development and evaluation of the various SBAM processes was carried out with the same starting powder. While the powder can be fed directly to the molding (pressing) in the conventional powder metallurgical process route, technology-specific pre-material developments are necessary for the sinter-based AM processes. This is also shown in Table 2 and described in more detail in the process descriptions. After sintering, microstructure and mechanical properties were investigated.

Table 2: Process chains of the evaluated sinter-based AM technologies from the starting powder to the finished sintered component compared to the conventional PM route for D185 (reference)

metal powder	starting material	shaping/compaction	debindering	sintering & HV treatment
reference: deagglomerated	metal powder	Conventional pressing (die / drybag pressing)	-	✓
this work: as reference plus additionally protective sieved to eliminate agglomerates	feedstock filament	Filament Material Extrusion F-MEX	✓	✓
	feedstock granules	Granules Material Extrusion G-MEX	✓	✓
	feedstock granules	Metal Selective Laser Sintering M-SLS	✓	✓
	feedstock block	Lithography-based Metal Manufacturing LMM	✓	✓
	metal powder	Metal Binder Jetting MBJ	✓	✓
	suspension	Mold Slurry Deposition MSD	✓	✓

Powder

The Densimet® D185 powder mixture was obtained with a standard mixing routine using high purity W, Ni, and Fe powders with average grain sizes of 4-5 µm each. Tungsten powder was supplied by Global Tungsten Powder (GTP®). Once mixed, milled and sieved to eliminate agglomerates with sizes >36 µm, the powder characteristics such as chemical composition, particle size distribution and powder tap density were determined and are summarized in Table 3. Morphology can be seen in the SEM images below (Fig. 1).

Table 3: Characteristic properties of the WHA powder mixture D185 with nominal composition (W-2Ni-1Fe)

	chemical composition and impurities					particle size distribution				density		
	W (wt.%)	Ni (wt.%)	Fe (wt.%)	C (µg/g)	O (µg/g)	d10 (µm)	d50 (µm)	d90 (µm)	d100 (µm)	theor. (g/cm^3)	tap (g/cm^3)	rel. tap (%)
measured	97.1	1.87	0.91	22	668	2.69	5.48	10.26	15.72	18.5	8.82	47.7

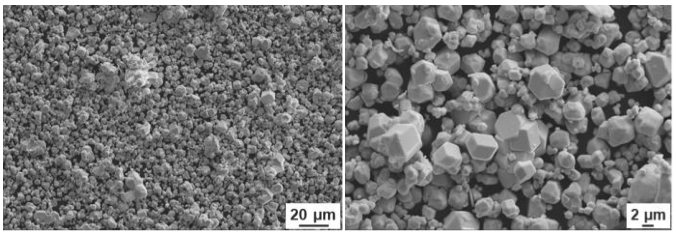

Fig. 1. SEM images of the powder mixture

Filament and Granules Material Extrusion (F-MEX and G-MEX)

The schematics and workflow of Material Extrusion technologies are shown in Fig. 2. A Metal Injection Moulding Feedstock with a powder loading of 55 vol.% metal powder was manufactured by mixing thermoplastic organic binder with the powder using a sigma blade kneader. In

the case of G-MEX the granules could be directly printed. For F-MEX a slight adjustment of binder composition was necessary to achieve sufficient flexibility for subsequent filament manufacture and winding the spool, while at the same time having as much rigidity as possible for the printing process. Filament with a target diameter of 1.75±0.05 mm was produced with a Collin Teachline Extruder using a nozzle diameter of 2.0 mm. The accuracy of the diameter was determined with an average value of 1.760 mm and a standard deviation of ±0.007 mm.

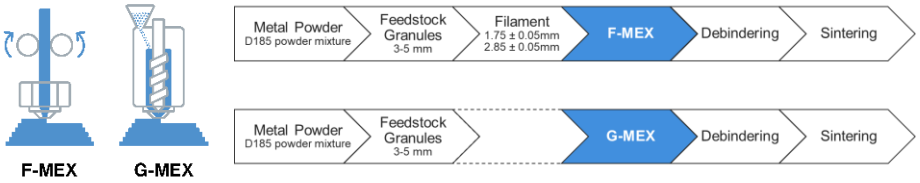

Fig. 2. Schematics and workflows of MEX technologies using filaments or granules

For both MEX processes, an extensive optimization of printing parameters, such as temperatures, mass flow, coasting and wiping, resulted in good green part quality with respect to the surface quality, green density, layer adhesion and green strength. The evaluation was carried out on printed bars of the size 5 x 5 x 35 mm³, as shown in Fig. 3. There, F-MEX green parts are shown before (top) and after (bottom) parameter optimization. Micrographs after sintering show the defects of the microstructural formation. In this case former voids are infiltrated by the Ni-Fe phase during the sintering process which can lead to a weakening of the material with respect to mechanical properties.

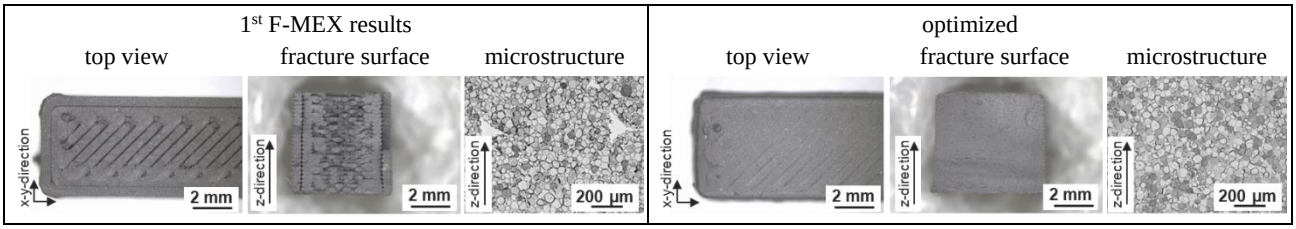

Fig. 3: F-MEX green part quality of D185 bars and microstructure after sintering
(top before and bottom after printing parameter optimization)

Metal Selective Laser Sintering (M-SLS)

Based on previous investigations with Densimet D176 [7], a feedstock with a granule size <160 µm consisting of metallic D185 starting powder and a proprietary thermoplastic binder was produced. The optimum powder loading with respect to processability of 50 vol.% was reached. The printing tests to optimize the M-SLS parameters were carried out using an EOS Formiga P110 SLS system. Cylinders with a diameter of 10 mm and a height of 5 mm were printed and further processing was carried out via a two-stage debinding process (chemical with solvent and thermal) and subsequent sintering. As a reference, green cylinders produced by die pressing of the SLS granules were also further processed via the same steps. The results of density measurement and microstructure investigations on the sintered samples are summarized in Fig. 5.

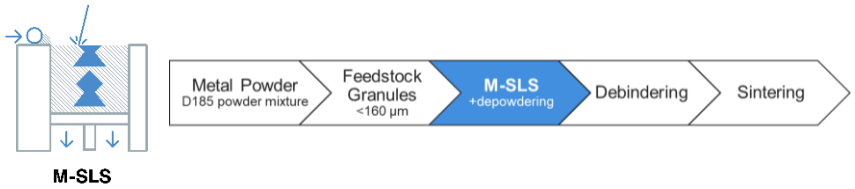

Fig. 4: Schematic and workflow of M-SLS technology

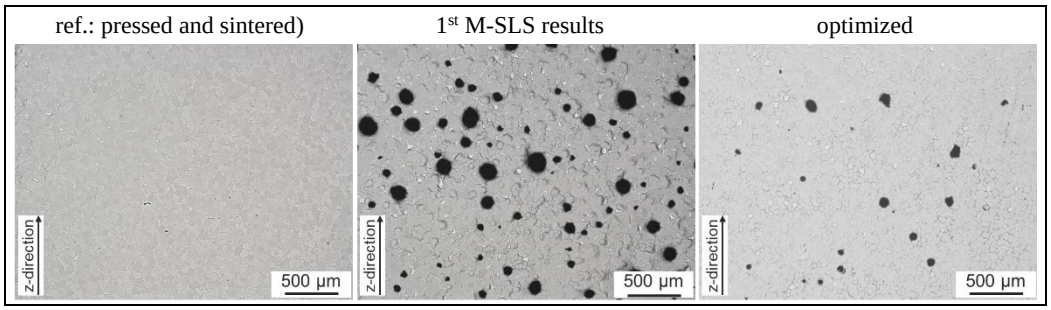

Fig. 5: Porosity of sintered WHA D185 samples manufactured by granule pressing (ref.)
and M-SLS printing (prior and after parameter optimization)

While the pressed cylinder could be sintered to 100% of the theoretical density and had a structure characteristic of this material (globular W

grains embedded in Ni-Fe matrix phase), the first sintered samples of the M-SLS process showed large pores that could not be closed despite liquid phase sintering. By optimizing the printing parameters such as recoating and laser parameters, temperatures, and printing strategies, density could be increased from 95% to 98%. With these parameters, bending beams, cylindrical tensile specimen blanks (upright and horizontal) and demonstrator parts were then printed.

Lithography-based Metal Manufacturing (LMM)

Fig. 6 shows the workflow of a LMM process. It was necessary to develop a D185 feedstock consisting of the D185 metal powder and a proprietary photopolymeric binder. This feedstock block contains a powder loading of 50 vol.% and polymerizes under UV radiation. Non-polymerized binder is then removed in a so-called decaking step, and the green part becomes further processed.

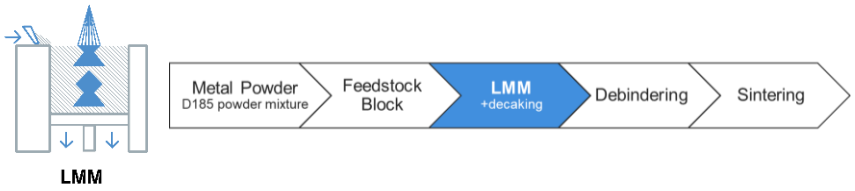

Fig. 6: Schematic and workflow of LMM technology

Parameter optimization for a layer height of 30 µm and a thermal treatment at elevated temperatures after decaking and cleaning resulted in green parts with a high accuracy, filigree details and a high green strength. Fig. 7 shows parts in the green and sintered state. Thermal debindering and sintering resulted in fully metallic and 100% dense parts. Optical micrographs of the cross section of the as-sintered state confirm the avoidance of residual porosity and show the typical microstructure of a liquid-phase sintered WHA.

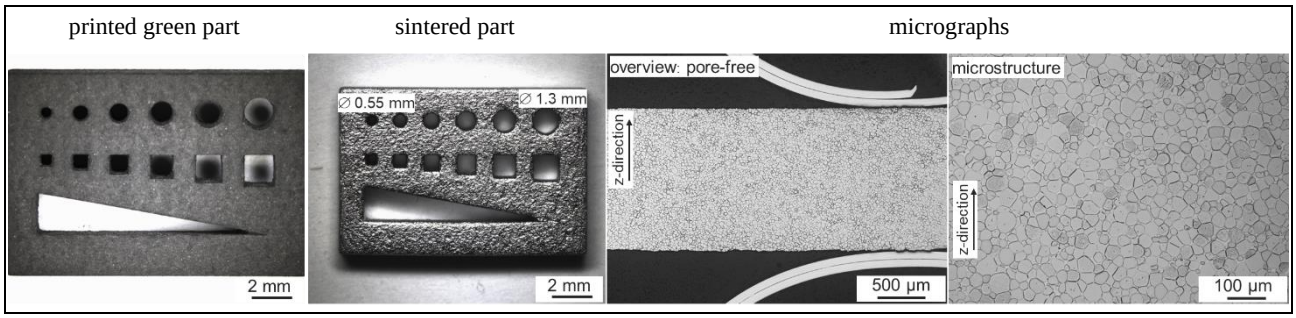

Fig. 7: WHA D185 part printed and fully dense sintered and cross-section micrographs of the sintered part

Metal Binder Jetting (MBJ)

The MBJ process (Fig. 8) is already well described in the literature and extensive studies exist for many materials [8-11]. The main influencing factors to produce metal parts by MBJ with consistently high quality are the sinterability of the processed metal powders, the sintering conditions themselves to avoid distortions, as well as the powder packing density in the green part [12].

The powder mixture used in this work is non-free-flowing, which is rather atypical for MBJ. Extensive parameter optimization for the printing process was carried out on an Innovent$^+$ system with the aim of achieving a high packing density, the highest possible green density with optimal component quality and edge sharpness.

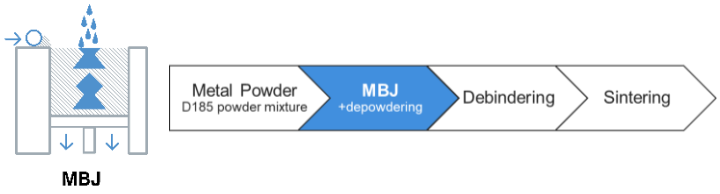

Fig. 8. Schematic and workflow of MBJ technology

With the water-based binder Aquafuse and a layer height of 40 µm (optimum for the powder), it was possible to produce green parts of high quality with respect to edge sharpness, surface, and level of detail. These green parts had a powder packing density of 46 vol.%, another 5 vol.% were organics. Thermal debindering and sintering using standard parameters for the powder resulted in fully dense parts with the typical WHA microstructure (Fig. 9).

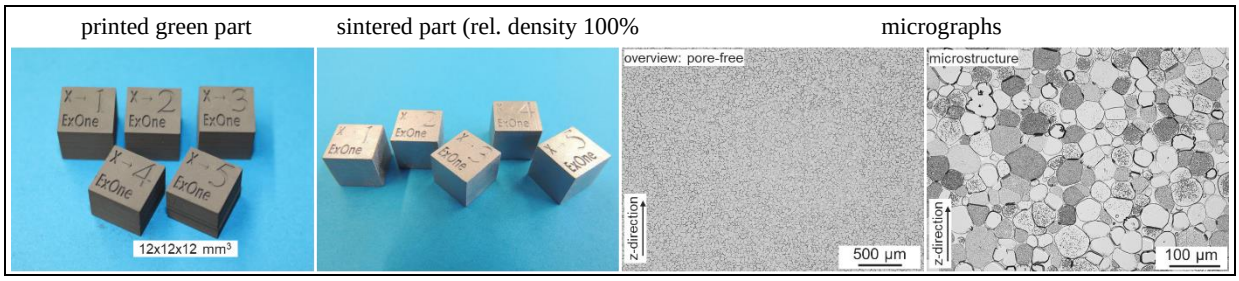

Fig. 9. WHA D185 parts printed and fully dense sintered and cross-section micrographs of the sintered part (cube design by Desktop Metal)

Mold Slurry Deposition (MSD)

MSD, also known as the MoldJet Process, is still a relatively young AM process. The printing principle described in the paper by Studnitzky et al. [5] is schematically depicted in Fig. 10, as is the workflow with upstream and downstream process steps.

Fig. 10. Schematic and workflow of MSD technology

For the evaluation of this AM technique, water-based slurry development for the WHA starting powder was carried out using a proprietary binder system. Improvements in the workflow of slurry preparation to avoid insertion of air bubbles (phase 1) and adjustments in the composition (phase 2: binder components, powder loading) resulted in a printable slurry. The processing of the developed slurry with a powder content of 45 vol.% and approx. 27 vol.% organics could be successfully demonstrated for layer heights of 50 and 100 µm, whereby the test specimens in Fig. 11 were produced with a layer height of 100µm. Density determinations as well as microstructural analyses of thermally debindered and sintered samples confirm the improvements of the individual development phases (Fig. 12).

Fig. 11. MSD printed D185 green parts (left: cubes 20x20x20 mm³ for slurry and workflow development; right: hexagonal beams with $\varnothing_i$ = 11 and L = 75 mm for mechanical testing in green and sintered state)

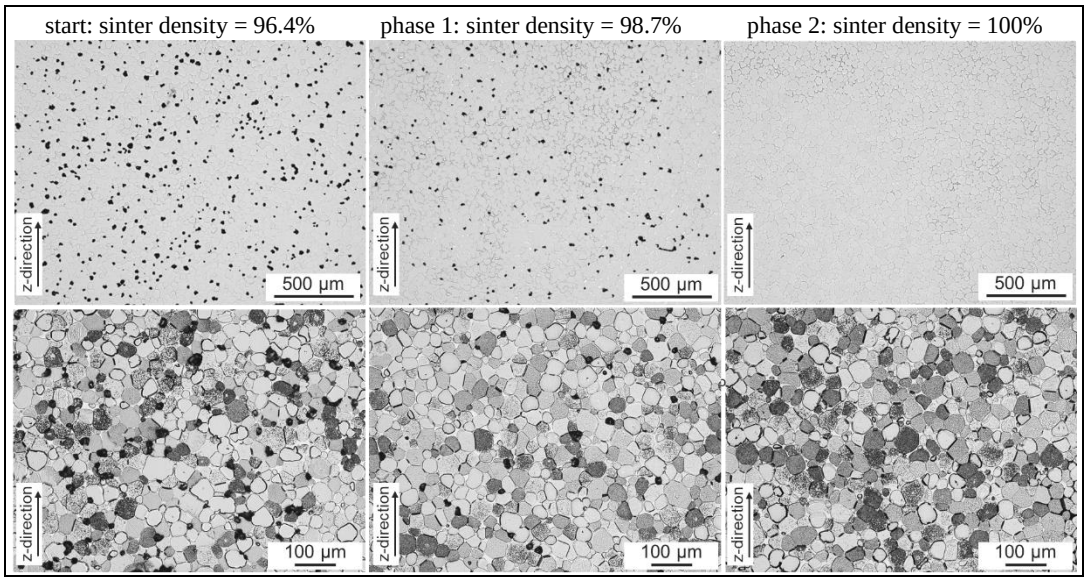

Fig. 12. Porosity and microstructure of sintered WHA D185 samples manufactured by MSD (depending on development phase)

Further processing and characterization

Three-point bending tests at room temperature using a ZwickRoell Z050 were carried out to determine the green strength after printing. The bending beams had a size of 4x4x25 mm³. The distance between the supports was 15 mm, the bending edge radius 1.5 mm and the radius of the supports 1 mm. The test speed was 1 mm/min.

Whereas conventionally pressed blanks can be fed directly into the sintering process, the printed parts via SBAM technologies have to undergo chemical and/or thermal debindering in a multi-step process. The thermal debindering is done under hydrogen at temperatures between 600 and 800°C. It needs to be set up in a way to process the parts without cracking while maintaining acceptable levels of impurities such as carbon (<300 µg/g) and sulfur (<4 µg/g). The subsequent sintering process corresponded to the standard solid-liquid sintering operation as is done for the conventional p/s route for WHA and was performed on alumina powder bed in pusher furnaces under temperatures between 1500°C and 1550°C. All sintered specimens were submitted to vacuum treatment to extract the hydrogen from the bulk. The shrinkage in the x, y and z directions of the print job was determined by geometric measurement of test specimens in the printed and sintered state. Density measurements, microstructure investigations and chemical analyses of residual carbon and oxygen contents were carried out to get information about the achievable component quality compared to the conventional production route (p/s).

Cylindrical tensile test samples with 5 mm diameter were machined from vacuum treated blanks of reference material (p/s) as well as SBAM routes. Tensile tests were performed under constant rate of 5 mm/min at room temperature. For some SBAM technologies values were only available in x-y direction, while for others also in z direction. Table 4 compares the test results with the minimum requirements of the WHA material class according to ASTM standard B777-15 and typical achievable values of the conventional route (p/s).

Table 4: Overview of green part compositions and the achieved test results for the SBAM processes in comparison to typical values of conventional powder metallurgical production (p/s) of sintered parts made of WHA D185 and to minimum requirements of ASTM standard B777-15 for this material class (n.d. – not determined)

	ASTM B777-15	conv. p/s	F-MEX		G-MEX		M-SLS		LMM		MBJ		MSD	
composition of green parts in vol.%														
powder	-	67	55		55		55		50		46		45	
binder	-	0	45		45		45		50		5		27	
porosity	-	33	0		0		0		0		49		28	
green strength determined by three-point bending test in MPa (test force parallel to the printing direction)														
average	-	n.d.	27.5		23.6		12.0		21.7		8.8		1.2	
standard dev.	-	n.d.	2.6		3.8		0.7		2.3		0.8		0.4	
sinter density determined by Archimedes principle, absolute in g/cm³ and relative in %														
absolute	18.25-18.85	18.52	18.52		18.52		18.06		18.52		18.52		18.52	
relative	-	100	100		100		98		100		100		100	
linear sintering shrinkage depending on the print directions x, y and z in %														
x	-	-	19.4		19.6		18.6		18.5		21.2		18.9	
y	-	-	19.4		19.5		18.6		18.5		21.9		19.0	
z	-	-	20.0		20.1		19.9		20.9		26.9		20.1	
residual carbon and oxygen contents after sintering in µg/g														
C	-	< 25	8		< 5		11		< 5		< 5		< 5	
O	-	< 20	10		< 5		6		< 5		< 5		< 5	
mechanical properties at room temperature, determined in tensile tests (⊥ perpendicular and ∥ parallel to the printed z-direction)														
			⊥	∥	⊥	∥	⊥	∥	⊥	∥	⊥	∥	⊥	∥
YS in MPa	> 517	735	745	745	734	742	727	710	739	773	735	n.d.	n.d.	n.d.
TS in MPa	> 758	985	1039	1039	1012	1025	982	844	1037	1035	1000	n.d.	n.d.	n.d.
A in %	> 2	15.0	16.6	11.0	15.2	12.1	13.5	11.5	19.0	18.0	13.7	n.d.	n.d.	n.d.

The results of the investigations carried out so far show that the green strengths are strongly influenced by the binder content determined by the SBAM-technology. This is particularly important in the production of very fine, filigree structures as well as in the handling of green parts. Except for M-SLS, the standard solid-liquid sintering operation of p/s WHA D185 resulted in fully dense components. With the achieved

sintering density of 100%, they meet the minimum requirements of the WHA ASTM specification. The formed microstructures correspond to those of the conventional p/s route as can be seen in Fig. 13. For M-SLS, further optimizations need to be made to increase sinter density and reduce residual porosity.

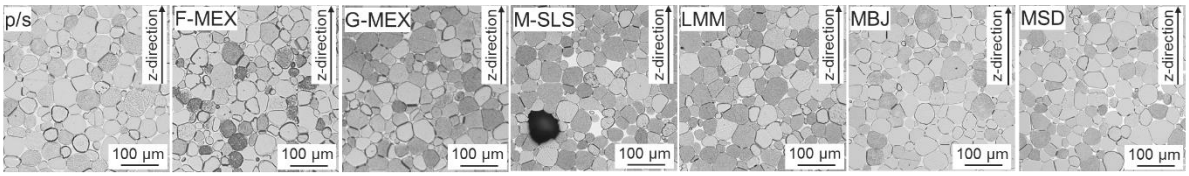

Fig. 13. Microstructures of sintered D185 samples of the investigated SBAM technologies in comparison to conventional material

The shrinkage of the SBAM sinter specimens shows slightly increased values in the z-direction compared to the values in x- and y-directions. An increased shrinkage anisotropy in MBJ is striking. It is assumed that this is caused by an increased porosity between the individual layers when the powder is applied.

Due to the tight process control in thermal debindering and sintering, low impurity contents of residual carbon and oxygen could be achieved for all SBAM technologies in this work. The final vacuum treatment to remove hydrogen made it possible to achieve the shown mechanical properties of the sinter parts. The microstructure and mechanical properties of WHA D185 are at the level of the conventional production and thus significantly above the minimum requirements of the ASTM specification. For MBJ in z-direction and for MSD, the values have not yet been determined. However, similar values are to be expected here.

Demonstration of feasibility

First WHA D185 prototypes and demonstrators of various sizes were successfully produced using the described process routes (Fig. 14). The feasibility of complex internal structures, the possibility to produce shell-like components or the potential of realizing very fine, thin-walled, filigree details in small and large quantities are to be demonstrated. The possibility of final machining is demonstrated here using the example of the MEX processes and the M-SLS, where post-processing ensures the achievement of the required surface qualities and tight tolerances, where they are needed.

Fig. 14. SBAM manufactured WHA D185 prototypes and demonstrator parts
(*design by Incus, ** design by © CULTS PU/ designer: ZERTUX [13])

Summary and classification of the results

Selected SBAM methods were examined for their suitability to process WHA. The processability of typical element powder mixtures consisting of 97 wt.% W, 2 wt.% Ni and 1 wt.% Fe, which are also processed in conventional production via pressing/sintering, was demonstrated. After the development and optimization of the corresponding starting materials and the process development for printing and debindering, it was possible to manufacture full-metallic components with outstanding properties through the subsequent use of standard solid-liquid sintering operation and a final vacuum treatment. Except for the M-SLS specimens and the still pending determination of mechanical properties for the MSD process, the sintered parts clearly meet the minimum requirements of ASTM standard B777-15. The feasibility considering process-specific limitations (e.g. resolution, accuracy, wall thicknesses, de-powderability, design rules) as well as the machining to achieve tight tolerances and high surface qualities was demonstrated on the first prototypes and demonstrators. Finally, findings about advantages and disadvantages, as well as limitations in the process workflow are shown in Table 4 to give an overview on the applicability of the evaluated

SBAM methods for WHA powders. Assessments from Studnitzky's preliminary work [5] as well as the results of this work are considered. When using this table, it must be mentioned that the individual evaluation of SBAM technologies is very much driven by the corresponding materials and by the specific applications of the printed products.

Table 5: Comparison of the examined SBAM methods according to selected criteria, considering the results of the investigations obtained; symbols and the individual assessment of the authors stand for trends and tendencies

	material choice & availability	size & weight	parts quantity	max. wall thickness	resolution & accuracy	feasibility of internal structures	green strength & robustness	mechanical properties	TRL of the process chain	time to market
F-MEX 	+ + (high)	+ (medium)	- (low)	O (moderate)	- (low)	+ + (given)	+ + (high)	+ + (very good)	+ (considerable)	+ + (close)
G-MEX 	+ + (high)	+ (medium)	- (low)	O (moderate)	- (low)	+ + (given)	+ + (high)	+ + (very good)	+ (considerable)	+ + (close)
M-SLS 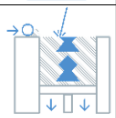	O (moderate)	+ (medium)	+ (considerable)	O (moderate)	- (low)	O (moderate)	+ + (high)	+ (good)	O (moderate)	+ (near)
LMM 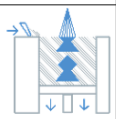	O (moderate)	- (tiny)	+ (considerable)	- (slim)	+ + (high)	+ (potentially)	+ + (high)	+ + (very good)	O (moderate)	+ (near)
MBJ 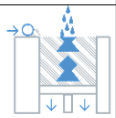	O (moderate)	O (small)	+ + (high)	+ (thick)	+ (considerable)	O (moderate)	O (moderate)	+ (good)	O (moderate)	O (moderate)
MSD 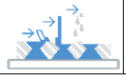	- (limited)	+ (medium)	+ + (high)	+ (thick)	+ (considerable)	+ (potentially)	- (low)	+ (good)	- (low)	- (far)

References

1) C. LIA, Y. WANG, S. MA, X. YANG, J. LI, Y. ZHOU, X. LIU, J. TANG, X. WANG, G. LE: International Journal of Refractory Metals & Hard Materials, 91 (2020) 105254
2) A. IVEKOVIĆ, M. L. MONTERO-SISTIAGA, K. VANMEENSEL, J.-P. KRUTH, J. VLEUGELS: International Journal of Refractory Metals & Hard Materials, 82 (2019) 23–30
3) H. CHEN, X. ZI, Y. HAN, J. DONG, S. LIU, C. CHEN: International Journal of Refractory Metals & Hard Materials, 86, (2020) 105111
4) T. SCHWANEKAMP, A. MUELLER, M. REUBER, H. GOBRAN, N. GDOURA, S. VON CETTO: International Journal of Refractory Metals and Hard Materials, 109 (2022) 105959
5) T. STUDNITZKY, C. ZHONG, T. WEISSGAERBER, C. AUMUND-KOPP: Conference Paper of Euro Powder Metallurgy 2023 Congress & Exhibition, DOI:10.59499/EP235765077
6) ASTM International, Designation: B777 - 15 (2020)
7) C. STAUDIGL, C. FISCHER, D. HANDTRACK, M. SCHARVOGEL: Proceedings of Euro Powder Metallurgy 2021 Congress & Exhibition, 491-495
8) D. GODLINSKI, G. VELTL: Proceedings of Euro Powder Metallurgy 2005 Congress & Exhibition, Vol. 3, 49–54
9) J.A. GONZALEZ, J. MIRELES, Y. LIN, R.B. WICKER: Ceramics International, 42 (2016) 10559–10564
10) R.K. ENNETI, K.C. PROUGH, T.A. WOLFE, A. KLEIN, N. STUDLEY, J.L. TRASORRAS: International Journal of Refractory Metals and Hard Materials, 71 (2018) 28–35
11) A. MOSTAFAEI, E.L. STEVENS, E.T. HUGHES, S.D. BIERY, C. HILLA, M. CHMIELUS: Materials & Design, 108, (2016) 126–135
12) B. BARTHEL, S. HEIN, F. PETZOLDT: Proceedings of Euro Powder Metallurgy 2019 Congress & Exhibition
13) ©CULTS PU: https://cults3d.com/en/3d-model/art/fly-zertux